

Basin-scale motion in stratified Upper Lake Constance

Jochen Appt¹

Institut für Wasserbau, Universität Stuttgart, Pfaffenwaldring 61, D-70550 Stuttgart, Germany

Jörg Imberger

School of Water Research, Centre for Water Research, University of Western Australia, Crawley, 6009, Western Australia, Australia

Helmut Kobus

Institut für Wasserbau, Universität Stuttgart, Pfaffenwaldring 61, D-70550 Stuttgart, Germany

Abstract

This paper describes experimental and modeled wind-induced oscillations in Upper Lake Constance with an emphasis on a coherent understanding of the basin-scale internal dynamics in this example of a large and stratified lake. Data were collected with eight Lake Diagnostic Systems (LDSs) consisting of thermistor chains and wind anemometers. The isotherm displacements as measured by the LDSs were interpreted using the three-dimensional hydrodynamic Estuary and Lake Computer Model (ELCOM). Three types of basin-scale waves were found to dominate the wave motion: the vertical mode-one Kelvin wave that had an observed period around 90 h, two vertical mode-one Poincaré waves that had periods near 8 h and 12 h, and a vertical mode-two Poincaré wave that had a period near 14 h. After strong westerly winds, upwelling of cold bottom water was observed east of the Sill of Mainau, where the lake's two subbasins connect. The width and length ratios of the subbasins, spatial variations of the wind field, and rotational effects over the lake are shown to play critical roles in the details of the upwelling structure. A sudden fall of the isotherms in Lake Überlingen formed a surge. The reflection of the surge from the northwestern boundary induced a vertical mode-two response leading to an intrusion in the metalimnion that caused a three-layer velocity structure in the smaller subbasin.

The energy path transferring mechanical energy from the wind down to the smallest scales of motion begins with the baroclinic basin-scale motions (Imberger 1998). In the present study, field work and three-dimensional numerical modeling were integrated to develop a coherent picture of basin-scale baroclinic motions in Upper Lake Constance, Europe, as an example for a large stratified lake with complex topography, responding to some moderate and severe wind episodes during a period of strong cooling. The term basin-scale denotes motions with length scales that are fixed by the basin topography. The study is an example for the possible extent to which numerical methods after proper validation and field measurements may be combined in order to

gain a more coherent understanding of the behavior of large stratified lakes.

Upper Lake Constance is used for drinking water supply for about four million people, for recreational purposes, and for commercial fishery (Fig. 1). Its basin has a length of 63 km and a maximum width of 14 km. Motions along the talweg will be referred to as longitudinal, while transverse motions are perpendicular to the talweg. Two subbasins form the lake: the larger subbasin is the main basin with a maximum water depth of 252 m and a mean depth of 101 m; the smaller subbasin of Lake Überlingen has a maximum water depth of 147 m and a mean depth of 84 m (reviewed in Wessels 1998). The mean width of the main basin is 9.3 km, while Lake Überlingen has a mean width of 2.3 km. The subbasins are connected at the Sill of Mainau, where the depth at the talweg reduces to 100 m. The seasonal density stratification is primarily due to the temperature, with salinity having an effect only when temperatures are near 4°C (Ollinger 1999). The prevailing synoptic-scale winds come from the southwest–west (SW–W) and northeast (NE). The former winds prevail particularly during strong wind events that occur on 2–9 d per month and have a duration between 1 and 7 d (Huss and Stranz 1970). A mountain ridge south of Lake Überlingen leads to smaller wind magnitudes over Lake Überlingen when the wind direction is SW–W (Zenger et al. 1990). Periodically, foehn winds flow down from the south along the Alpine Rhine valley and influence the eastern main basin (Mühleisen 1977).

¹ Corresponding author (Jochen.Appt@appt.de).

Acknowledgments

This research was conducted with financial support of the Deutsche Forschungsgemeinschaft (KO 528/17); the Institut für Wasserbau, Universität Stuttgart; and the Centre for Environmental Fluid Dynamics, University of Western Australia. The collaboration of Erich Bäuerle, Frank Molkenhain, Karl-Otto Rothhaupt, Gerd Schröder, as well as of many more supporting persons, was instrumental in the success of the field measurement program. Special thanks go to the Centre for Water Research (CWR) field operation group for their contribution to the field work and to Dorothee Schweizer for ensuring an efficient computer environment. Helpful discussions and support are particularly acknowledged from Ben R. Hodges concerning the ELCOM model as well as from Bernard Laval, Jason Antenucci, Simone Mödinger, and Leon Boegman regarding the data analysis. The authors would like to thank the reviewers of this paper for constructive suggestions.

Basin-scale internal waves—Basin-scale internal waves in Upper Lake Constance are significantly affected by the

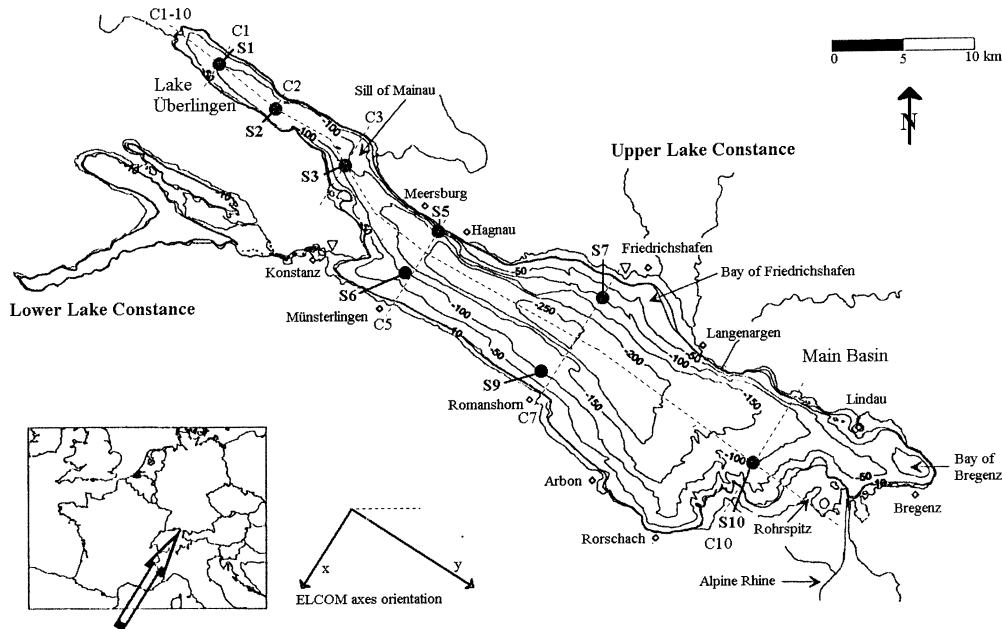


Fig. 1. Upper Lake Constance (47°39'N, 9°18'E) bathymetry with locations of LDS sampling stations of the 2001 field program (index S). Locations of vertical transects (index C) for flow visualization are indicated as dashed lines. (Original map courtesy of Martin Wessels.)

earth's rotation, as is indicated by the Burger number S_i , i.e., the ratio of the internal Rossby radius R_R to a horizontal length scale L_s (Antenucci and Imberger 2001). For a typical thermal stratification as observed in autumn

$$R_R = \frac{c_1}{f} = \frac{0.3 \text{ m s}^{-1}}{1.07 \times 10^{-4} \text{ s}^{-1}} \approx 2800 \text{ m} \quad (1)$$

where c_1 is the two-layer estimate for the nonrotational baroclinic phase speed, which may be defined, for example, as by Mortimer (1952):

$$c_1 = \sqrt{g \frac{\rho_h - \rho_e}{\left(\frac{\rho_h}{h_h} + \frac{\rho_e}{h_e}\right)}} \quad (2)$$

where g is gravity, ρ is density, h is layer depth, and the indices e and h define the upper and lower layer, respectively. The inertial frequency at Upper Lake Constance is f . Defining L_s as half of the respective mean subbasin width yields $S_i = 0.6$ for the main basin and $S_i = 2.4$ for Lake Überlingen. The basin-scale internal wave response is therefore modified by the rotation into Kelvin-type waves, Poincaré-type waves, and topographic waves. Kelvin waves propagate along the shoreline with the shore to the right on the northern hemisphere (Mortimer 1974). Poincaré waves have periods less than the local inertial period of 16.3 h, and the associated velocity field rotates anticyclonically, i.e., clockwise on the Northern Hemisphere (Antenucci et al. 2000).

The horizontal uninodal vertical mode-one Kelvin wave is the most pronounced baroclinic signal in Upper Lake Constance (Bäuerle et al. 1998). Observed oscillation periods in autumn range between 90 and 120 h, with typical thermocline displacements of around 5–10 m in Lake Überlingen

and smaller displacements in the eastern end of the main basin (Zenger et al. 1989; Schimmele 1993; Bäuerle et al. 1998). Bäuerle (1981) showed that the observed Kelvin wave can be modeled reasonably well with a simple two-layer configuration referred to as the Bäuerle model in the following. Available field data were too sparse, however, to verify the propagation of the wave crest around the shoreline (Schimmele 1993).

Poincaré vertical mode-one waves in Upper Lake Constance have a more local character (Wang et al. 2000), with periods in autumn typically around 12 h in the central and eastern main basin (Hollan 1974; Heinz 1995; Wang et al. 2000), 9 h at the western end of the main basin (Heinz 1995; Wang et al. 2000), and 4 h in Lake Überlingen (Hollan 1974; Bäuerle 1994; Wang et al. 2000). Little seems to be known about basin-scale internal waves of higher vertical modes.

Response to strong wind forcing—Surface upwelling of cold bottom water is frequently observed in the western part of Upper Lake Constance during periods when winds with speeds greater than 5 m s^{-1} come from the SW–W (Hollan 1974; Zenger et al. 1989; Heinz 1995). The most extreme upwelling of cold water from depths down to 50 m was recorded at the northern shore in the main basin east of the Sill of Mainau where the subbasins connect, while upwelling at the upwind end of the basin, i.e., in Lake Überlingen, was observed to be less pronounced. The factors for this unusual upwelling structure have not been clarified. Little seems to be known about the initial response to wind forcing in large lakes that consist of two subbasins with different dimensions, even though there are other examples where upwelling has been observed, e.g., in Lake Biwa, Japan (Hayami et al. 1996). In a lake with no rotation, the relative strength of the

forcing can be parameterized with the dimensionless lake number (reviewed in Imberger and Patterson 1990) as

$$L_N = \frac{M_{bc}}{M_{wind}} \quad (3)$$

where M_{bc} and M_{wind} are the baroclinic moment and the moment due to wind surface stress, respectively, about the center of volume (see Eq. 7 for details). Low lake numbers ($L_N \ll 1$) are associated with upwelling of the thermocline to the surface at the upwind end of the lake. In contrast, in large lakes Csanady (1982) showed that upwelling will be observed on the shore 90° to the left of the direction in which the wind is blowing.

Strong downward movement of the metalimnion can generate nonlinear internal surges (e.g., Thorpe and Hall 1972; Mortimer and Horn 1982; Lemmin 1987; Hayami et al. 1996). These may be characterized as nonlinear Kelvin waves propagating as progressive waves of depression with approximately the linear phase speed (Thorpe and Hall 1972). The evolution of internal surges in Upper Lake Constance was observed after strong upwelling, but again field data were too sparse to allow full understanding (Hollan 1974; Schimmele 1993; Heinz 1995). Observed internal surges in autumn were characterized by two abrupt falls of the thermocline, the first of which propagated to the western end of the lake with velocities of $0.2\text{--}0.3\text{ m s}^{-1}$, i.e., close to the linear phase speed (Zenger 1989; Schimmele 1993; Boehrer et al. 2000). At a location just east of the Sill of Mainau, the thermocline fall was observed to be up to 60 m over about 3 h. Associated horizontal velocities measured near the bottom reached 0.14 m s^{-1} in 190 m depth in the main basin (Heinz 1995). Typically, the isotherm fall was followed by a second, well-defined fall in Lake Überlingen after the surge had been reflected at its northwestern basin end (Zenger 1989; Schimmele 1993; Boehrer et al. 2000). This phenomenon of two consecutive thermocline falls in Lake Überlingen will be called two-step thermocline in the following. From a review of measurements associated with the two-step thermocline we may conjecture that the second fall may be linked to the three-layer velocity structure reported by Boehrer et al. (2000). These authors measured velocity vectors in the metalimnion of Lake Überlingen that were directed toward the main basin and in the opposite direction from the velocities in the epilimnion and hypolimnion.

This study is an example of how an existing three-dimensional numerical model and field measurements can be combined in order to obtain a more coherent understanding of the lake motion as a basis for understanding the lake ecosystem. Measurements of water temperature and wind velocities from eight on-lake stations and one full meteorological station on the lake were analyzed in order to construct a coherent understanding of the interplay of individual phenomena of the lake response to meteorological forcing. A spatiotemporally distributed wind field and surface heat fluxes were used to force the numerical model. Investigated phenomena include internal waves of the Kelvin and Poincaré type, an upwelling event of bottom water to the surface, internal surges, and an intrusion in the metalimnion of Lake Überlingen associated with a three-layer velocity structure.

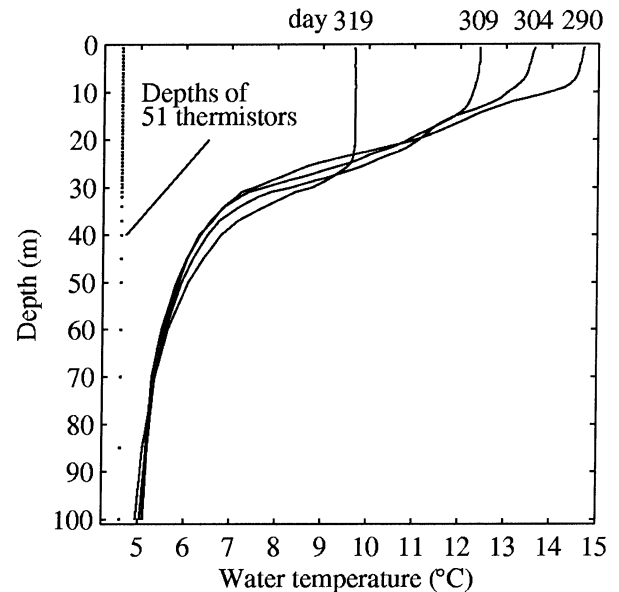


Fig. 2. Vertical temperature profiles of daily averaged field data at S7. The time of each profile is written on top of that profile. Dots at 4.6°C indicate the depth distribution of thermistors.

Methodology

Field experiment—The temperature distributions of the water column and the wind at the water surface were measured in 2001 over 33 d from day 288 of the year through day 321 (15 October–17 November). Eight Centre for Water Research (CWR) Lake Diagnostic Systems (LDSs) were moored at locations shown in Fig. 1. Each station was equipped with a single-cable thermistor chain of 100 m length, as well as with a wind anemometer and a wind direction sensor located at 2.4 m height above the water. Each thermistor chain consisted of 51 thermistors with an accuracy of 0.01°C and a resolution of 0.001°C . The thermistors were placed at 0.75-m intervals in the upper 30 m and at increasing intervals of 1.00 to 15.00 m below as shown in Fig. 2. In addition, a meteorological station at station S7 recorded relative air humidity, air temperature, incident short wave radiation, and total net radiation. Samples were collected at 10- or 30-s intervals.

The wind, temperature stratification, and meteorological conditions during the experiment were typical for autumn and comparable to previous measurements in 1972 (Hollan 1974) and 1993 (Heinz 1995). The measurement period was characterized by two periods with different wind and surface cooling characteristics: during period I, from day 288 through day 310, the daily air temperature was approximately constant to day 304, after which it plunged to a little over $+7^\circ\text{C}$ (Fig. 3a). Weak and moderate wind with an average speed of 2.1 m s^{-1} (Fig. 3b) induced small-amplitude internal wave seiching (Fig. 3c,d). Surface water temperatures decreased from 15°C to 12°C (Fig. 2). At the beginning of period I, the surface mixing layer was approximately 10 m deep (Fig. 3c). The metalimnion was marked by a linear temperature decrease between 10 and 40 m, below which

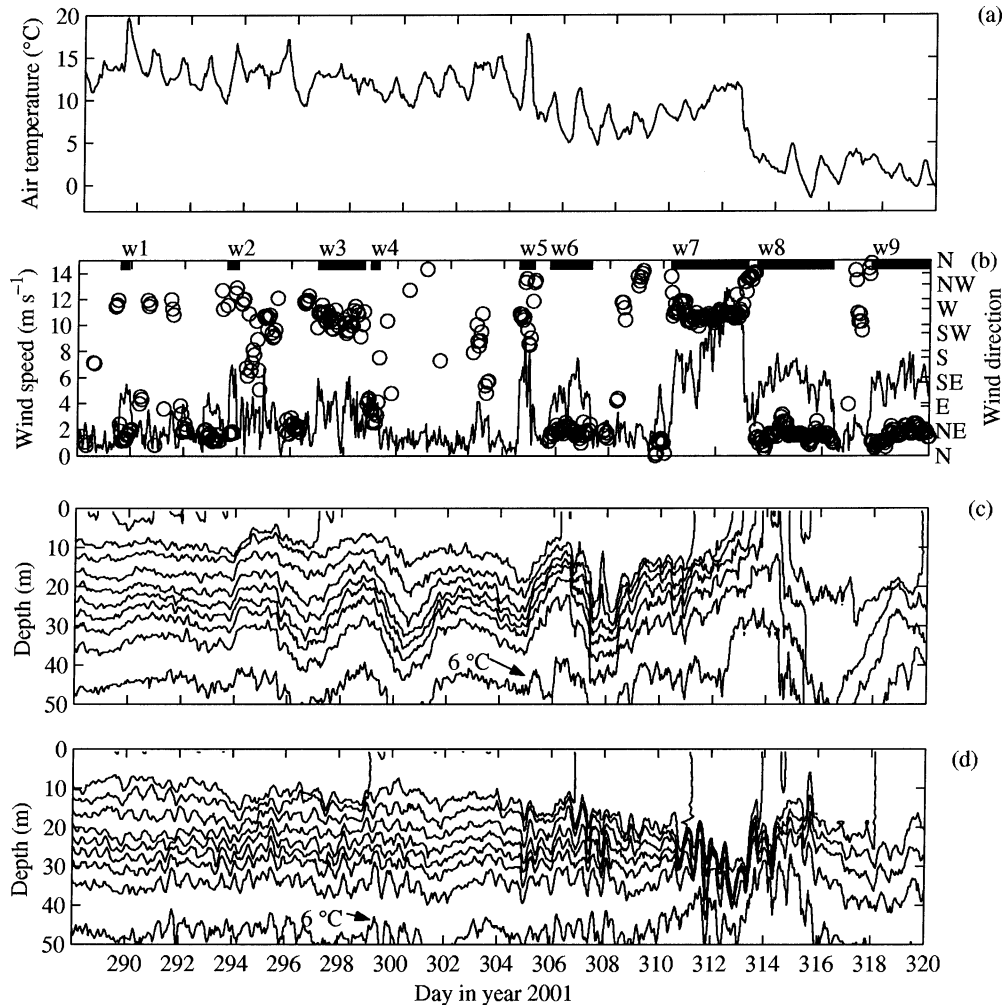


Fig. 3. Examples of field data in the main basin and in Lake Überlingen: (a) 1-h average of air temperature at Sta. S7 in 2.11 m height above the water surface; (b) 1-h averages of wind speed and direction at S7 in 2.4 m height. Wind direction plotted as circle when speed exceeded 2 m s^{-1} , horizontal bars and numbers w1–w9 denote individual wind events. (c) 1-h average of isotherm response at S2, the bottom isotherm is 6°C , with a 1°C contour interval; (d) same as in panel c for S9.

temperature decreased slowly throughout the hypolimnion to 4.6°C at the bottom.

Period II on day 311 was marked by a strong west-southwest (WSW) wind event (w7 in Fig. 3b), a rapid fall in air temperature to below $+4^\circ\text{C}$, and a drop of the surface water temperature. The WSW wind event at the beginning of period II led to wind speeds of 14 m s^{-1} causing upwelling in the western part of the lake (Fig. 4a–d, day 313) and downwelling in the eastern part of the main basin (Fig. 4h, day 313). Upwelling in the western part set up an internal surge noticeable from the abrupt thermocline fall on day 314 (Figs. 3c and 4a–d). The propagation of the reflected internal surge is marked by a second fall of the isotherms in the lower metalimnion and their return between day 315 and day 316 (Figs. 3c and 4a–d).

Typical winds from the north-northeast–east-northeast (NNE–ENE) and the southwest–northwest (SW–NW) were observed most frequently during the measurement (Fig. 5).

The occurrence of winds reflects the wind shadowing over Lake Überlingen, e.g., during the WSW breeze w7 the daily averaged wind speed on day 312 was 5.4 m s^{-1} over Lake Überlingen at S2 and 9.6 m s^{-1} over the main basin at S7. The wind direction from the SW–NW was pronounced at all stations, while the NE direction was particularly pronounced in the western and central part of the main basin (e.g., S7). Foehn winds from southern directions were observed in the eastern main basin (S10).

Numerical simulation—Simulations were performed with the CWR Estuary and Lake Computer Model (ELCOM), code version 1.5, which has been shown to model successfully the baroclinic dynamics of stratified lakes (Hodges et al. 2000; Laval et al. 2003). The code solves the three-dimensional Navier–Stokes and scalar transport equations separating mixing of scalars and momentum from advection and making use of the hydrostatic and Boussinesq assumptions

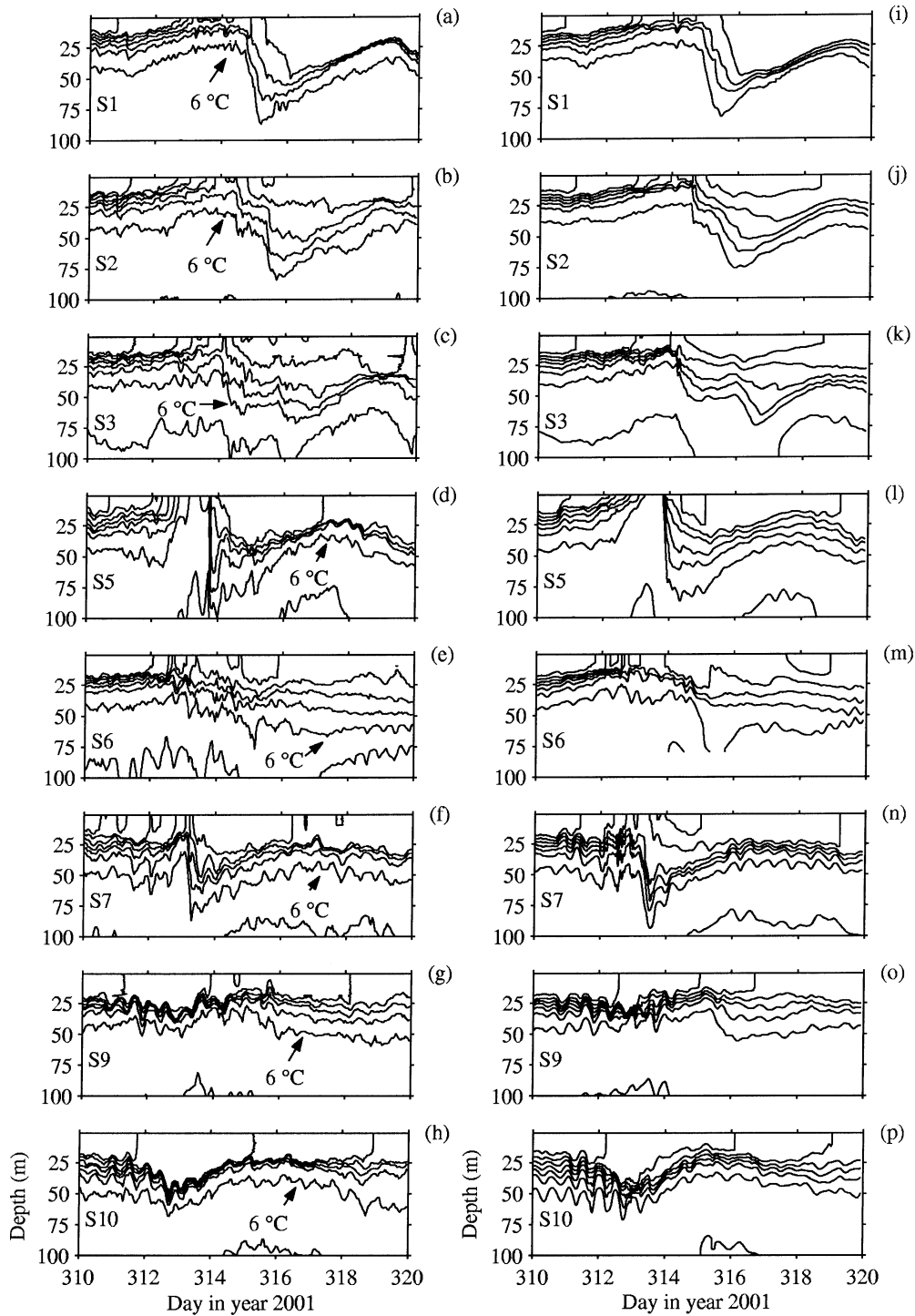


Fig. 4. Isotherm displacement during and after strong WSW breeze starting on day 310: (a–h) 1-h averages of field data; (i–p) 240-s interval model results. The first contour lines above the station names represent the 6°C isotherm. Isotherms with 1°C contour interval.

(Hodges and Dallimore 2001). The cumulative effects of numerical diffusion are reduced with a potential energy preserving recursive filter applied immediately after the momentum calculation at each time step (Laval et al. 2003). The model was applied to Upper Lake Constance without specific calibration of model parameters. A uniform hori-

zontal grid with a mesh size of 400 m was used with the orientation of the coordinate axes as indicated in Fig. 1. Vertical grid sizes varied gradually between 2.5 m down to the hypolimnion and 34 m near the deepest part of the lake. On boundary faces, the velocity was assumed to be free-slip. The model was initialized with a horizontally uniform tem-

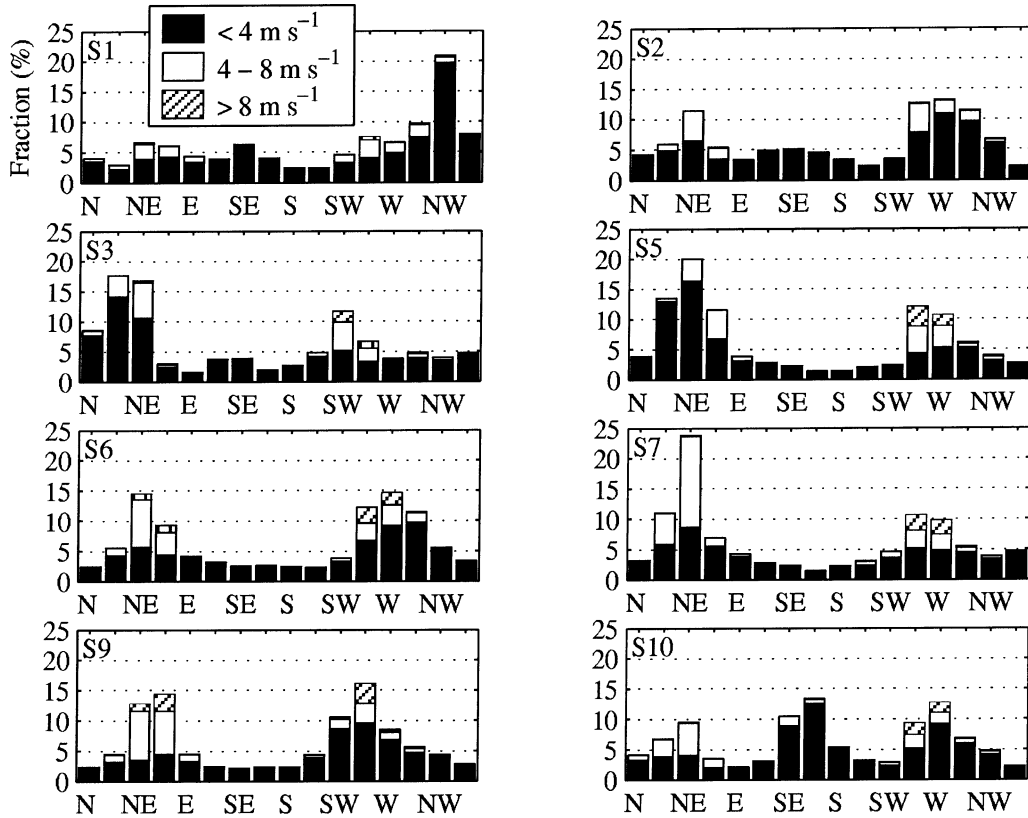


Fig. 5. Occurrence of 10-min averaged wind speeds at different stations in 2.4 m height above the water surface between day 288 (15 October, 1800 h) and day 320.25 (16 November, 0600 h). Direction defined as bins of 22.5°.

perature profile, a horizontal free-surface, and zero velocity everywhere. The simulated period covers days 292.0–320.0 with a time step of 240 s.

Stress at the surface boundary due to wind was modeled as a momentum source distributed evenly over the homogeneous surface layer. The wind field over the water surface was constructed from an interpolation of the measured wind at the lake stations, averaged over the simulation time step, to the surface of each numerical water column. Measured wind speeds were adjusted to the 10-m reference elevation assuming a simple neutral meteorological boundary layer

$$U_{w10} = \frac{\ln\left(\frac{10.0 \text{ m}}{z_0}\right)}{\ln\left(\frac{2.4 \text{ m}}{z_0}\right)} U_{w2.4} = 1.14 U_{w2.4} \quad (4)$$

where $U_{w2.4}$ and U_{w10} are the wind speeds at 2.4 and 10 m height. The equation $z_0 = 1.15 \times 10^{-4} \text{ m}$ is an estimate of the roughness height of the water surface. In this study, first-order variations of the wind field have been considered, such as the wind shadowing effect over Lake Überlingen. The model validation shows that the model results, and thus the choice of z_0 , are acceptable for this purpose. Future investigations may improve the model results by reducing uncertainties such as the atmospheric stability. Surface heat fluxes

were computed from measured air temperature, relative humidity, wind speed, cloud cover, and incoming short wave radiation using the standard bulk aerodynamic formulation of ELCOM.

Basin-scale internal wave field

Theoretical velocity structure—The vertical modal structure corresponding to the average density profile between day 289 and day 293 at Sta. S10 (Fig. 6a) was estimated from a normal mode decomposition (Antenucci et al. 2000) assuming a flat bottom and the average basin depth of 100 m. This assumption seems justified, since the calculation is not very sensitive to variations of depth if temperature profiles are extended. The equation for the vertical velocity w_n (Kundu 1990) is

$$\frac{d}{dz} \left(\frac{1}{N^2} \frac{dw_n}{dz} \right) + \frac{1}{c_n^2} w_n(z) = 0 \quad (5)$$

where c_n is the phase speed of the n th vertical mode. The vertical mode-one oscillation is characterized by a phase speed $c_1 = 0.29 \text{ m s}^{-1}$ and largest isotherm displacement amplitudes at a depth of about 25 m (Fig. 6b). The vertical mode-two oscillation has a phase speed of $c_2 = 0.12 \text{ m s}^{-1}$ and largest isotherm displacement amplitudes in the upper and lower part of the metalimnion (Fig. 6c). In order to

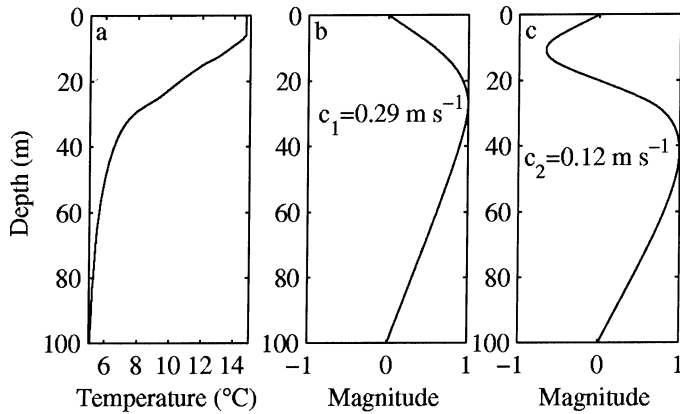


Fig. 6. Vertical modal structure. (a) Background temperature stratification between day 289 and day 293 at S10; (b) vertical mode-one eigenfunction for vertical velocity w for the stratification in panel a; (c) vertical mode-two eigenfunction.

estimate the sensitivity of the results to depth variations, the same calculation was done for a depth of 200 m. This increases the phase speed by about 10%.

Frequency content of motion—The frequency content of the integrated potential energy (PE) per unit area of the water column was analyzed using a power spectral method (Bendat and Piersol 1971). Only the upper 100 m of the water column were considered for this calculation, which includes the region with a significant temperature gradient. The PE signal selects the vertical mode-one components of the signal preferentially relative to higher vertical modes (Antenucci et al. 2000). Time series of PE were calculated from the density stratification by

$$\text{PE}(t) = \int_{z_r}^H \rho(z, t)gz \, dz \quad (6)$$

where $H = 100 \text{ m}$, ρ is the water density due to temperature, t is time, z is the vertical coordinate positive upward, g is gravity, and $z_r = 0$ is the reference elevation. During period I there was an increased spectral density around 90 h at all stations (Fig. 7a, solid lines) corresponding to the basin-scale vertical mode-one Kelvin wave. The increase was most pronounced at Stas. S1, S2, and S3 in Lake Überlingen. Another statistically significant peak occurred at 12 h ($2.3 \times 10^{-5} \text{ Hz}$), particularly at S10, S9, and S7. At Stas. S6 and S5 this peak had shifted to a period of 8 h ($3.5 \times 10^{-5} \text{ Hz}$). This energy peak corresponded to a vertical mode-one Poincaré wave, the period of which Wang et al. (2000) has previously shown to be dependent on the station location. The spectra from the model results are also shown in Fig. 7a (dotted lines), which shows that ELCOM successfully reproduced the vertical mode-one Kelvin and Poincaré wave energies and frequencies. This result is similar to that already noted in the Lake Kinneret simulations by Hodges et al. (2000). During period II only the Poincaré wave at Stas. S7, S9, and S10 was statistically significant (Fig. 7b), the main basin-scale waves being overwhelmed by the forced motions (*see below*).

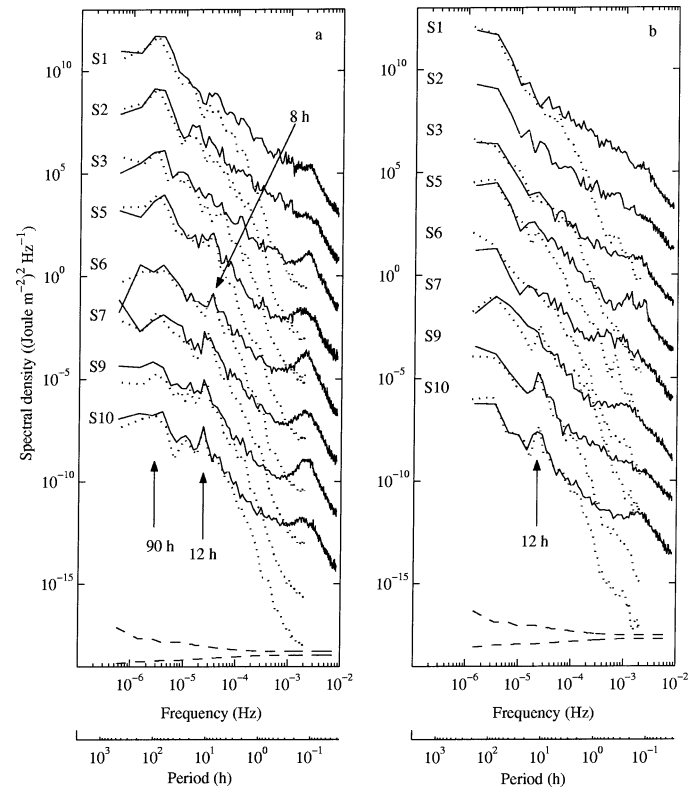


Fig. 7. Spectral analysis of field (solid lines) and simulated data (dotted lines). (a) Spectra of PE for simulated data as well as for 1-min averaged field data of the interval days 288.0–310.0 for S1, S2, S3, S7, and S9, days 293.0–310.0 for S6 and S10, as well as days 288.0–306.0 for S5; (b) same as in panel a for period days 310.0–320.0 at all stations. Confidence at the 95% level shown by the dashed lines. Coordinates of spectra staggered between adjacent stations.

The frequency content and rotation of the simulated velocity field was determined through rotary spectral analysis of isopycnal velocities (Gonella 1972; Antenucci et al. 2000). The 12.0°C, 9.0°C, and 5.5°C isotherms represent the lower epilimnion, the center of the metalimnion, and the hypolimnion, respectively (Fig. 2). An example of typical spectra of the main basin is presented in Fig. 8 for the velocity at the 9.0°C isotherm, i.e., in the metalimnion, illustrating the particularly strong energy peak around 14 h, which will be shown to belong to a vertical mode-two oscillation. Other spectra of velocities in the epilimnion and in the hypolimnion (not shown) confirm that the 12-h and the 8-h oscillations, i.e., vertical mode-one, also have in common an anticyclonically (clockwise) rotating velocity field.

Kelvin wave—As indicated above, the increased spectral density around 90 h is the signal of the Kelvin wave. Its counterclockwise travel along the shoreline is evident from the excursion of the metalimnion that is represented by the 9°C isotherm (Fig. 9c). The travel history is more clearly seen from band-passed PE variations shown in Fig. 9d with the internal crests labeled 1–6 and internal troughs labeled a–e. The phase speed around the main basin, from Sta. S6 to Sta. S5, is almost constant, as indicated by the linear pro-

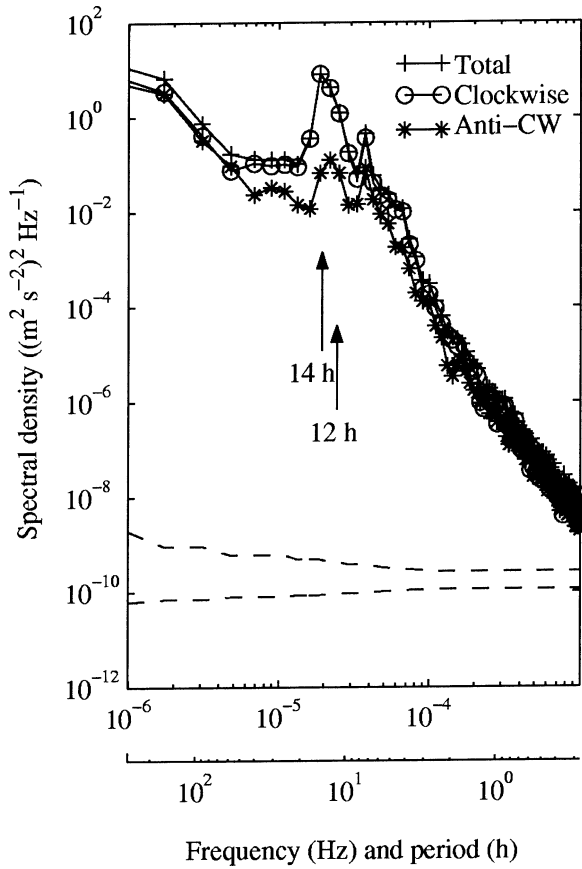


Fig. 8. Rotary power spectra of isopycnal velocity, decomposed into clockwise and anticlockwise rotating components of 9.0°C isopycnal velocity at S7. Model data of the velocity field between day 293.0 and day 310.0. Line markers show Fourier frequency discretization with spectra smoothed in the frequency domain. Confidence at the 95% level shown by the dashed lines.

gression of the crests and troughs. Observed periods vary between 72 and 105 h with an average of 90 h. The crests steepen when they pass Sta. S5 and enter Lake Überlingen through the contraction and over the Sill of Mainau. Given a finite amplitude, this steepening leads to a surge formation that moves the warmer surface water into Lake Überlingen. This is evident from the arrival of crest 5 when an abrupt thermocline fall was observed in the order S3, S2, and finally S1 (Fig. 9c). In Fig. 10a an expanded plot shows how the surge passed Sta. S2 on day 306.65 traveling westward toward S1, reaching it on day 306.85. Upon reaching the boundary, the surge reflected and returned eastward toward the main basin, passing S1 on day 307.16, S2 on day 307.37, and S3 on day 307.65. Parts of this surge formation, propagation, and reflection were documented previously by Holan (1974), Schimmele (1993), and Heinz (1995).

The simulated Kelvin wave signal plotted in Fig. 9d (dashed lines) shows a delay of some hours. The wave attenuation during the calm period (crest 4 and troughs c and d) is stronger in the simulated than in the measured data, possibly indicating that the steplike topography in the model retards the momentum too much (Gomez pers. comm.). Bäuerle's basin mode model yielded a Kelvin wave eigen-

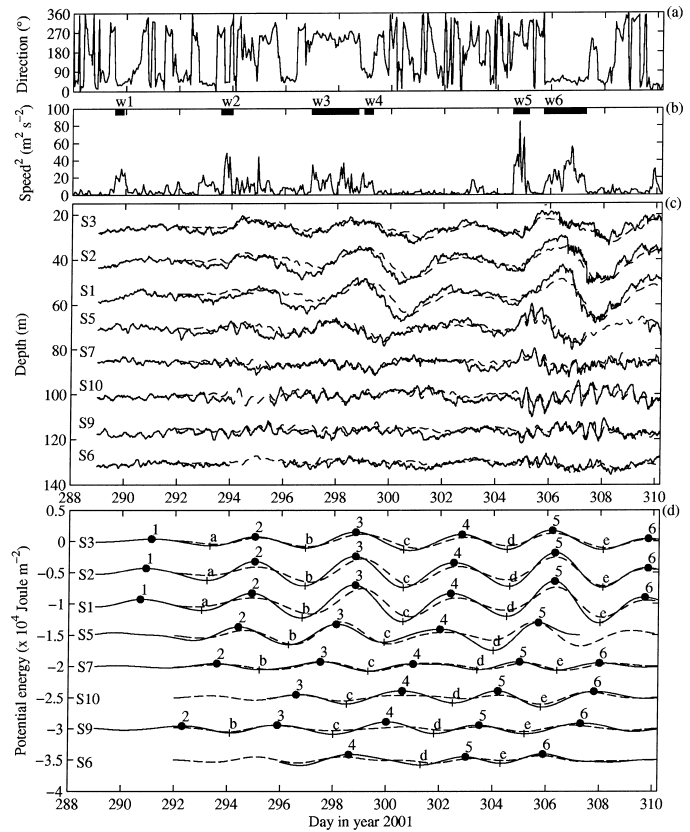


Fig. 9. Measured 1-h averages at S7 of (a) wind direction; (b) wind speed squared. Horizontal bars and numbers w1–w6 denote individual wind events; (c) 9°C isotherms staggered at 15-m intervals. 10-min averaged field data (solid lines) and 4-min ELCOM model results (dashed lines). (d) Butterworth-filtered time series (limits: 60–200 h, fourth order) of PE. The time series of PE are staggered with dots denoting the wave crests 1–6, and + denoting wave troughs a–e.

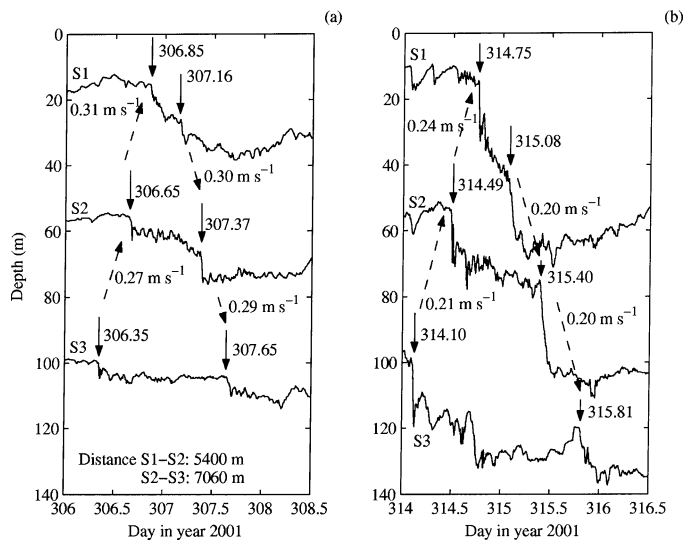


Fig. 10. Isotherm displacement after two wind episodes from the western direction at S1, S2, and S3: (a) 9°C isotherms from 10-min averaged field data; (b) 7°C isotherms from 1-h averaged field data. Depth plotted with 30-m shift between adjacent stations.

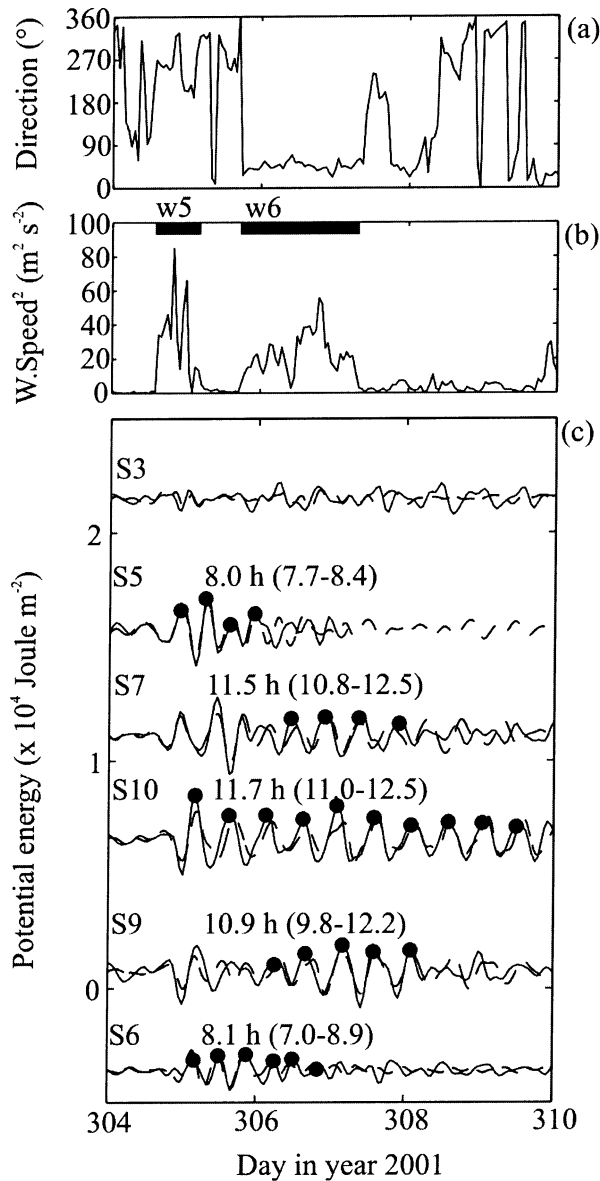


Fig. 11. Measured 1-h averages at S7 of (a) wind direction; (b) wind speed squared. (c) Butterworth-filtered time series (limits: 4–18 h, sixth order) of PE variations. The dots denote local maxima that were used for calculations. Field data (solid lines) and ELCOM model results (broken lines).

function period of 109 h (Bäuerle pers. comm.), which was very similar to that obtained with an ELCOM simulation that was forced with an impulsive wind lasting for 1 d and no wind afterward (108 h, not shown). By comparison, the observed Kelvin wave period (Fig. 9d) in the field was closer to 90 h. This suggests that direct wind forcing may have been responsible for the periodical resetting or at least modification of the free Kelvin wave, thus forcing an apparent smaller period.

Poincaré-type waves—The dominant 12-, 8-, and 14-h oscillations are of Poincaré wave type. The 12-h oscillation is observable in Fig. 9c (e.g., on day 306) at S10, S9, and S7.

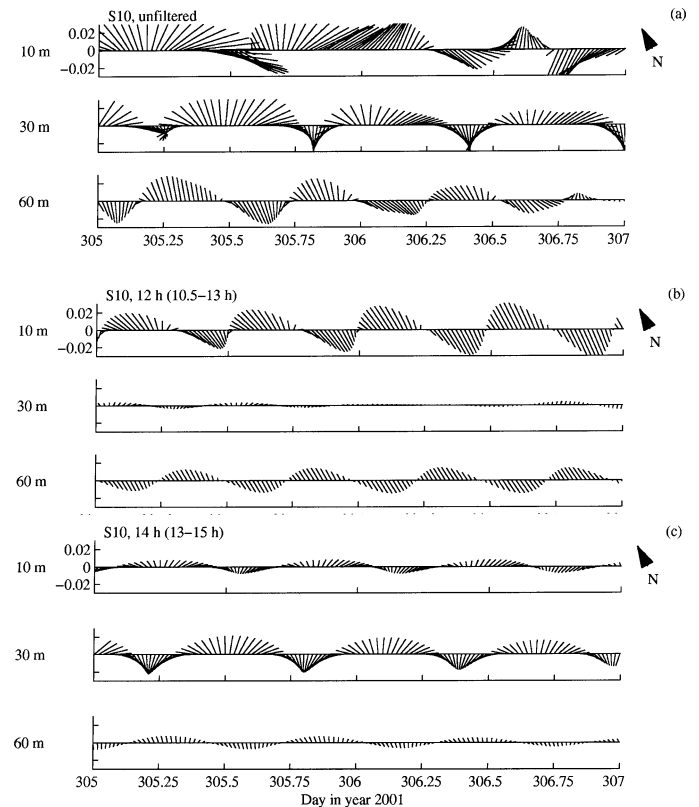


Fig. 12. Simulated velocity field at S10. Time series of horizontal velocity vectors from ELCOM simulation plotted for three depths: (a) unfiltered, (b) band-pass filtered (limits: 10.5–13.0 h), (c) band-pass filtered (limits: 13.0–15.0 h). Ordinate is day in 2001, coordinate is velocity in m s^{-1} .

Details of the period between day 304 and day 310 are shown in Fig. 11 as the band-passed time series of PE. The signal was particularly clear at S10 after the onset of winds w5 and w6. Vertical excursions of the upper and lower metalimnion were in phase and largest near the center of the metalimnion (Fig. 3d, day 307), suggesting a vertical mode-one oscillation. The 12-h signal is particularly well captured by ELCOM at S10, where the phases and amplitudes are quantitatively reproduced for more than 5 d (Fig. 11) with a mean phase deviation from field data of less than 1.2 h. The simulated velocity field at S10 (Fig. 12a) was used to identify the vertical structure of the velocity field. Time series of velocity in three depths are presented, i.e., in the epilimnion (10 m), metalimnion (30 m), and hypolimnion (60 m), respectively. Band-pass filtering of the simulated velocity field around the 12-h period (Fig. 12b) suggests a vertical mode-one structure of the oscillation. In a similar way, the 8-h oscillation in the western main basin, particularly at S5 and S6, was identified as an oscillation of the vertical mode-one Poincaré wave type (not shown). The 14-h oscillation is dominant in the simulated velocity field of the main basin but not in the temperature signal (see Fig. 11). Filtering the velocity around the 14-h period (Fig. 12c) suggests a vertical mode-two structure at S10. At other stations in the main basin, the vertical mode-two structure is

Table 1. Upwelling of the 9°C isotherm to the water surface. The parameter t_0 is defined as the time when the measured water temperature in 0.75 m depth fell below 9°C, and t_{\min} is the time when the lowest surface temperature γ_{\min} was recorded.

Station	t_0 (d)	t_{\min} (d)	γ_{\min} (°C)
S1	313.1	314.8	8.0
S2	313.6	314.1	7.6
S3	313.7	314.1	7.8
S5	312.5	313.3	5.4
S6	313.3	313.3	9.0
S7	313.1	313.1	8.5

not as clear, possibly indicating the involvement of even higher vertical modes.

Response to strong wind forcing

As shown in Fig. 3a, the weather became progressively cooler over the study period, and on day 310 the strong WSW breeze w7 marked the beginning of period II, with maximum wind velocities of 12 m s⁻¹ (Fig. 3b) on day 313. This strong westerly wind imparted momentum to the surface layer water, subtracting momentum from the Kelvin wave and finally moving the surface layer eastward from Lake Überlingen into the main basin. Fig. 4a–h shows measured isotherm displacements during and after the breeze. The time t_0 when upwelling of the 9°C isotherm was to the surface at S1, S2, S3, S5, S6, and S7 is given in Table 1. Upwelling of bottom water to the surface commenced not at the upwind end of Lake Überlingen but at S5 on day 312.5 (Fig. 4d), i.e., at the northern shore east of the Sill of Mainau when the 9°C isotherm in Lake Überlingen was still 12–14 m below the water surface (Fig. 4a–c). At the end of the breeze, on day 313.3, the minimum surface water temperature $\vartheta_{\min} = 5.4^\circ\text{C}$ was measured at S5 again. Corresponding downwelling caused the 9°C isotherm to fall to a depth of 30–40 m in the eastern main basin (Fig. 4h). The metalimnion was also tilted about the longitudinal lake axis downward toward the southern shore, implying a net transport of the surface layer water to southern directions, i.e., opposite to the transverse wind shear stress component. Figure 13 shows the spatial temperature structure along the longitudinal basin axis sketched from field data: colder water east of the sill split the surface layer over the whole width of the lake, particularly near the northern shore.

Figure 4i–p shows simulated isotherm displacements during upwelling. The basin-scale response, the cooling of the water column, and the upwelling are quantitatively reproduced. Figure 14 shows the simulated vertical temperature structure along one longitudinal (C1–10, indicated in Fig. 1) and six transverse (C1, C2, C3, C5, C7, C10) transects. The transects on day 313.17 show the split surface layer and the transverse tilt of the thermocline. Model results suggest that wind-induced horizontal water velocities near the surface during the breeze w7 were significantly smaller in Lake Überlingen than in the main basin due to wind shadowing. For example, on day 312.4, i.e., during the strongest wind forcing, the simulated average longitudinal velocity in 2.5 m

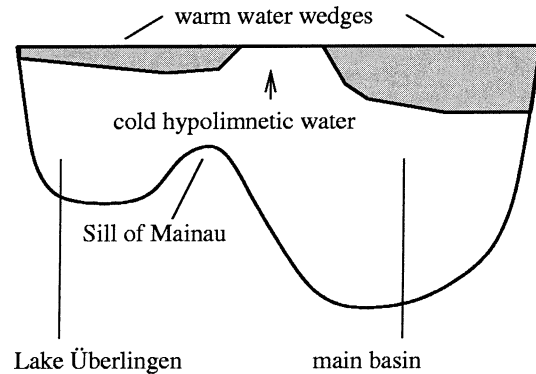


Fig. 13. Schematic of thermal structure of upwelling during westerly strong breeze.

depth was 9 cm s⁻¹ along the transect C2 in Lake Überlingen and 18 cm s⁻¹ along C7 in the main basin. The difference in the wind drag therefore caused different horizontal volume fluxes per unit width of the transects. Total volume fluxes through the transects differed even more due to the smaller width of Lake Überlingen. The total volume fluxes were estimated from simulated data assuming a two-layer structure and using the 9°C isotherm as a dividing line between the upper and lower layer. Longitudinal volume fluxes through the respective layers in transect C2 were $Q_U = 1.7 \times 10^3 \text{ m}^3 \text{ s}^{-1}$ and $Q_M = 11.4 \times 10^3 \text{ m}^3 \text{ s}^{-1}$ through C7; i.e., the total volume flux in the upper layer in the main basin was significantly larger than in Lake Überlingen.

In conclusion, the observed upwelling structure is characterized by the most extreme upwelling occurring at the northern shore east of the Sill of Mainau, while a layer of warmer surface water remains in Lake Überlingen.

Longitudinal force balance—The lake number concept was applied in order to evaluate the relative strength of the longitudinal wind component of wind w7 based on the temperature stratification of day 309. Upwelling to the surface is defined here as the intersection of the 9°C isotherm with the water surface. Equation 3 can be extended (Imberger and Patterson 1990) as

$$L_N = \frac{S_t(z_s - z_T)}{u_*^2 A_s (z_s - z_v) 0.5L} \quad (7)$$

where the length scale $A_s^{0.5}$ of the original lake number definition is replaced by $0.5 \times L$, which is half of the basin length. The parameter z_s is the height of the water surface, z_T is the height of the seasonal thermocline that was assumed to be located in 25 m depth, z_v is the height of the center of volume, and A_s is the surface area of the lake. The stability of the vertical water column is defined as

$$S_t = \frac{g}{\rho(z_s)} (z_s - z_g) m \quad (8)$$

where $\rho(z_s) = 999.97 \text{ kg m}^{-3}$ is the water density at the surface, z_g is the height of the center of gravity, and m is the mass of the water body. The shear velocity component

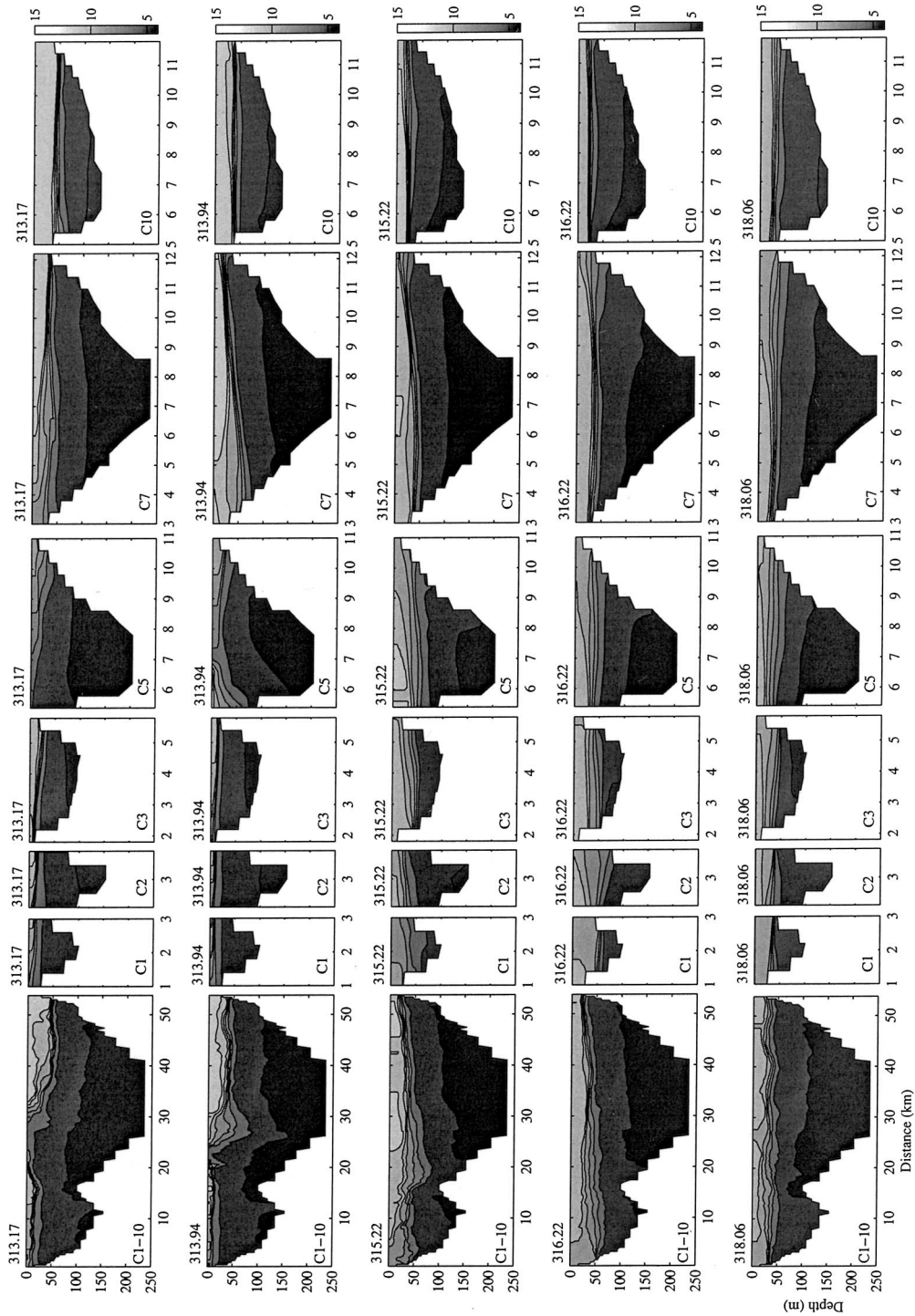


Fig. 14. Thermal structure along longitudinal (C1–10) and transverse vertical transects (C1, C2, C3, C5, C7, C10). Each row presents the transects at a certain time, each column a certain transect. Transverse transects plotted with the northern shore on the left. The time (day of the year 2001) is noted at the top of each figure. A gray scale bar of temperature (in °C) is included on the right.

along the longitudinal lake axis is given by

$$u_*^2 = \frac{\rho_{air}}{\rho_0} C_D U_{w10}^2 \cos \alpha \quad (9)$$

where $\rho_{air} = 1.2 \text{ kg m}^{-3}$ is the density of air, $C_D = 1.5 \times$

10^{-3} is the wind drag coefficient, and $\alpha = 55^\circ$ (i.e., for WSW) is the angle between the wind direction and the longitudinal lake axis. The wind speed U_{w10} at the reference level 10 m above the water surface on day 312 was near 10 m s^{-1} . This lake number is then close to 1 assuming either

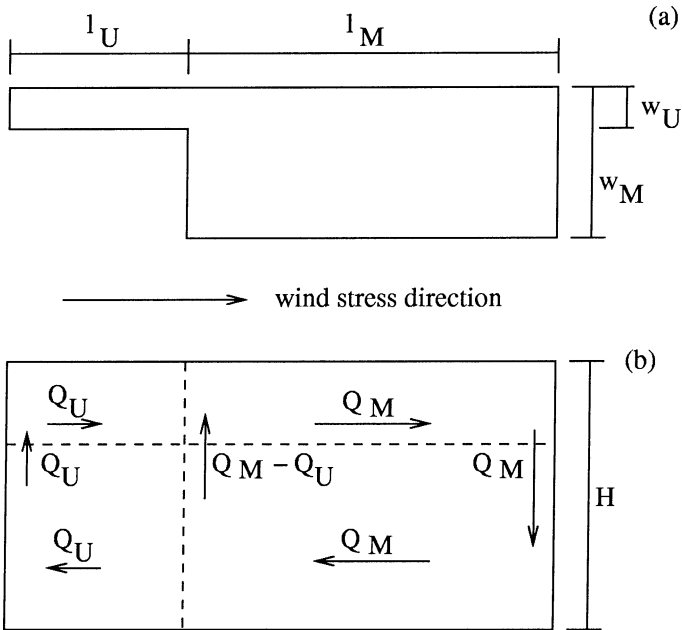


Fig. 15. Conceptual model of upwelling: (a) plan view of idealized basin of Upper Lake Constance; (b) vertical section with volume fluxes Q during upwelling. Indices M and U denote the main basin and Lake Überlingen, respectively.

a continuous tilt of the thermocline through the whole lake ($L = 63$ km) or a complete decoupling of the subbasins, calculating the lake number only for the main basin ($L = 47$ km). There was, thus, approximately enough wind momentum to cause upwelling of bottom water to the surface in the longitudinal direction.

Length and width ratios of the subbasins—Upwelling of bottom water occurs east of the sill while there is still warmer water in Lake Überlingen. In order to explain this first qualitatively, the lake basin may be idealized by two rectangular subbasins (Fig. 15). Rotation, mixing, and surface heat fluxes are not considered. The two-layered subbasins (upper layer depth h_1 , lower layer depth h_2 , $h_1 < h_2$) have equal total depths for simplicity ($H_M = H_U = H = h_1 + h_2$). The larger main basin has a length ($l_M = 47$ km) and width ($w_M = 9.3$ km) comparable to the main basin of Upper Lake Constance, and the smaller subbasin has the length of Lake Überlingen ($l_U = 16$ km) but a width w_U varying between zero and the width of the main basin ($0 \leq w_U \leq 9.3$ km). Wind shear stress is assumed to act uniformly along the longitudinal axis from the smaller subbasin toward the main basin. If the width of the smaller subbasin is infinitesimally small, there is no effect on the upwelling structure in the larger subbasin; full upwelling in the main basin will be that of a rectangular basin of length l_M . If the subbasins have the same width, the upwelling structure will be that of a simple rectangular basin of length $l_M + l_U$, with upwelling commencing at the upwind end of only the smaller subbasin and no split upper layer at the upwind end of the larger basin. The mean width ratio of Lake Überlingen and the main basin is 0.25; therefore, the actual behavior of the lake may be expected to be somewhere between these extremes.

In order to gain a quantitative understanding, the rigid-lid assumption is applied at the free water surface of the idealized basin with $w_U = 2.3$ km and the flow is averaged over the transverse direction. The principle of the volume conservation requires longitudinal volume fluxes in the upper layer across any transverse transect to equal the opposite compensation flux in the lower layer. Let Q_M be a representative forced volume flux for the main basin and Q_U for the smaller subbasin, assuming that the basin ends are distant enough to have no significant effect on these fluxes. If Q_U is smaller than Q_M , volume conservation requires that only part of the water from the lower layer of the main basin moves across the basin interface into the smaller subbasin. The remaining lower layer flux ($Q_M - Q_U$) in the main basin is deflected upward and replaces the upper layer flux Q_M that is driven away and that is not replaced by the smaller upper layer flux Q_U . The region of cold water near the surface then spreads toward the center of the main basin. A sill between the subbasins may support the upward deflection of the lower layer east of that sill, but the principle explanation of the phenomenon seems not to depend on its existence. This is important to note, since much attention was drawn previously to the sill alone (e.g., Kocsis et al. 1998). Two reasons for the assumed different volume fluxes are the smaller width of Lake Überlingen and the wind shadowing over Lake Überlingen. This wind shadowing effect also causes a smaller longitudinal tilt of the metalimnion in this subbasin compared to the main basin.

A further aspect is the length ratio of the subbasins. One may think of the case where the warmer surface layer moves out of Lake Überlingen into the main basin before upwelling to the surface commences east of the sill. At the time of full upwelling east of the sill, there would be cold water everywhere in Lake Überlingen and no split surface layer would be observed. To investigate the likelihood of this, it is assumed that the upper layer of Lake Überlingen moves as a slab of constant velocity toward the main basin. The time T_{removal} when the upper layer is removed from Lake Überlingen may be scaled by the length of Lake Überlingen $l_U = 16$ km divided by the simulated average speed of the upper layer in Lake Überlingen v_1

$$T_{\text{removal}} = \frac{l_U}{v_1} \quad (10)$$

The time for full upwelling to develop at the western end of the main basin may be scaled as one-fourth of the internal seiche period of the main basin; thus

$$T_{\text{upwell}} = \frac{1}{4} \frac{2l_M}{c_1} \quad (11)$$

Setting $T_{\text{removal}} > T_{\text{upwell}}$ yields a generalized condition for a split surface layer to be observed as

$$\frac{l_M v_1}{2c_1 l_U} < 1 \quad (12)$$

Using the above calculated $v_1 = 0.07$ m s⁻¹ as a velocity estimate for the upper layer, $l_M = 47$ km as the length of the main basin, and a phase speed of 0.3 m s⁻¹, Eq. 12 yields

Table 2. Transverse force balance.

	S5	S7
h_1 (m)	10	30
v_1 (m s^{-1})	+0.16	+0.20
$u_*^2 h_1^{-1}$ (m s^{-2})	-1×10^{-5}	-3×10^{-6}
fv_1 (m s^{-2})	1.7×10^{-5}	2.1×10^{-5}

a time ratio of 0.3. Thus, a split surface layer east of the sill may be expected.

Rotational effects—The earth's rotation causes the strongest upwelling at the northern shore east of the sill for a predominantly transverse wind component from the south-western direction, as can be demonstrated with a model run without Coriolis forces (not shown). In the real lake, the upper layer moved away from the northern shore opposite to the direction of the transverse wind stress component. As done by Csanady (1982), a three-layer fluid may be considered with the equilibrium depth of the upper layer h_1 and the vertical surface displacement η_1 . The x and y direction are defined as in Fig. 1, and the z -axis is positive upward. u_1 and v_1 are the velocities in the upper layer in the x and y direction, respectively. Supposing the pressure to be hydrostatic, the linearized equation of motion considering Coriolis forces for the upper layer in the x direction is

$$\frac{\partial u_1}{\partial t} - fv_1 = -g \frac{\partial \eta_1}{\partial x} + \frac{u_*^2}{h_1} \quad (13)$$

The force balance may be calculated for day 313.0 at Stas. S5 and S7. The transverse wind shear speed component was estimated as

$$\begin{aligned} u_*^2 &= 1.5 \times 10^{-6} (10 \text{ m s}^{-1})^2 \sin(55^\circ) \\ &= 1.2 \times 10^{-4} \text{ m}^2 \text{ s}^{-2} \end{aligned} \quad (14)$$

h_1 is defined as the water depth where the reversal of the modeled transverse velocity component occurred, and v_1 is the average velocity component in the upper layer. The results shown in Table 2 indicate that the acceleration due to the transverse wind stress momentum is smaller than the acceleration due to the Coriolis force. This can be balanced in Eq. 13 by a gradient of the surface displacement η_1 , which requires a prior movement of the upper layer away from the northern shore, i.e., against the transverse wind component. As long as there is no balance among these three terms there is an acceleration of the upper layer opposite to the wind stress. The scaling analysis confirms that the Coriolis force acceleration was in the same order or even larger than the transverse wind acceleration.

Internal surge and intrusion in the metalimnion

Upwelling in Lake Überlingen continued after the cessation of wind w_7 . For example, the upwelling of the 9°C isotherm at S3 did not occur before day 313.7 (Table 1). It can be shown by model runs without surface heat transfer that the surface cooling influenced the water temperature near the surface to some extent, but the overall picture of

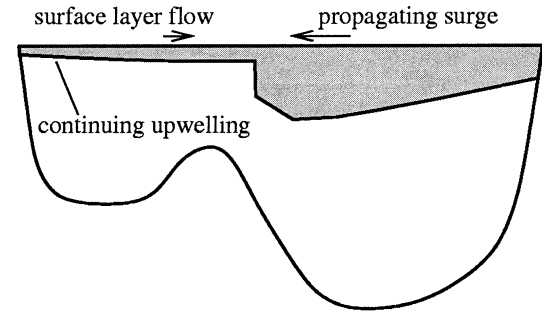


Fig. 16. Schematic of evolution of an internal surge.

the continuing upwelling remains. In contrast to the situation in Lake Überlingen, upwelling stopped in the main basin almost immediately after the cessation of the wind. The wedge of warmer surface water in the eastern main basin started to evolve into an internal surge, i.e., much in the way described by Thorpe (1974) for the internal surge in Loch Ness that begins when the thermocline, having previously been tilted, returns to the level position. The thermocline both in the eastern part of the main basin and in Lake Überlingen therefore moved upward while it fell at locations of preceding upwelling in the central part of the main basin (Fig. 16). As the surge approached the narrower and shallower western end of the main basin, its leading edge steepened. This agrees with the behavior of surges in Babine Lake (Farmer 1978), where a decrease in cross section increased the wave's amplitude while nonlinear effects associated with their finite amplitude steepened their leading edge. The strongest fall of the thermocline was measured at S5, where the 6°C isotherm fell from the lake surface to a depth of around 90 m within 2 h. This amplitude seems much larger compared to surges reported for other lakes (Hunkins and Fliegel 1973; Farmer 1978). The internal surge was associated with a reversal of the transverse tilt of the metalimnion falling toward the northern shore after the passage of the surge (Fig. 14).

The surge passed the Sill of Mainau in the morning of day 314. Its propagation in Lake Überlingen is marked by the first of two isotherm falls at S3, S2, and S1 (Fig. 10b). This passage of the surge was associated with unstable vertical temperature gradients (not shown). The propagation speed of this disturbance was $0.21\text{--}0.24 \text{ m s}^{-1}$, i.e., slightly more than the linear vertical mode-one phase speed of $c_1 = 0.16 \text{ m s}^{-1}$ at that time. In the evening of day 314, the internal surge arrived at the northwestern end of Lake Überlingen, and by the evening of day 315 water of medium density filled this basin end down to a depth of 50–60 m (Fig. 4a). Warmer water arriving from the main basin flowed on top of the medium-density water and forced the water of medium density to intrude into a layer being centered around approximately 50 m depth. The propagation of the reflected internal surge in the direction of the main basin is marked in Fig. 10b as the second fall of the two-step thermocline at S1, S2, and S3 between day 315 and day 316. The propagation speed of the reflected surge was 0.20 m s^{-1} , i.e., similar to the surge before the reflection. No clearly identifiable remnants of the reflected surge were apparent in the main

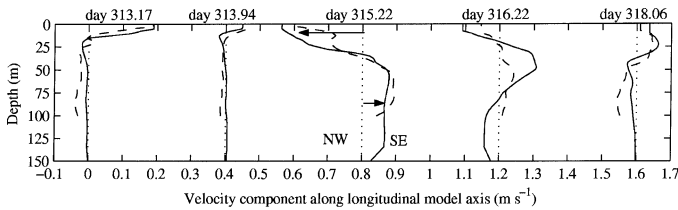


Fig. 17. Simulated horizontal velocity data plotted along longitudinal model axis at S2 (solid lines) and S3 (dashed lines). Staggered plot with an offset of 0.4 m s^{-1} between profiles.

basin, which is similar to records of Farmer (1978) in Babine Lake, where the signal of internal surges diminished as the cross section increased after passing a narrow.

It is remarkable that the already mentioned observation of the weak two-step isotherm around day 306 is very similar to the strong internal surge. As in the case of the strong surge, the reflected signal is not clearly identifiable in the main basin.

The comparison of simulated and field results in Fig. 4 shows that the model captures the evolution and propagation of the strong two-step thermocline associated with the internal surge after day 313 and its reflection at the northwestern end of Lake Überlingen. In the case of the weak surge, the numerical simulation underestimates the amplitude of the Kelvin wave and, thus, its nonlinear behavior. It can be demonstrated that the lack of a weak two-step thermocline in simulation results is not a principal insufficiency of the model but is clearly related to the already mentioned underestimated amplitude of the Kelvin wave.

Figure 14 shows validated model results for the arrival of the strong internal surge at the Sill of Mainau on day 313.94, the start of the reflection of the internal surge at the western end of Lake Überlingen on day 315.22, warmer water spreading on top of the water of medium density forcing the latter to intrude into southeast direction on day 316.22, and the propagation of an intrusion in the metalimnion to the southeast on day 318.06. Corresponding simulated longitudinal velocities at S2 and S3 are presented in Fig. 17.

When the strong internal surge reached Lake Überlingen, the preceding two-layer velocity structure in Lake Überlingen (Fig. 17, day 313.17) was reversed. After the surge passage water velocities near the surface reached more than $0.2\text{--}0.3 \text{ m s}^{-1}$ toward the NW (Fig. 17, day 315.22). At the same time, a strong current in the opposite direction evolved in the hypolimnion with speeds up to 0.1 m s^{-1} . There was, thus, essentially a two-layer velocity structure. This reversal of the two-layer velocity structure of Lake Überlingen on the arrival of the surge appears to be similar to the observation of Farmer (1978) in Babine Lake.

However, while the velocity in a depth of 30–50 m remained directed toward the main basin, there was another flow reversal in the hypolimnion of Lake Überlingen. This flow reversal was closely related to the propagation of the reflected internal surge that is marked by the second thermocline fall. This three-layer structure formed an intrusion with water in the middle layer in about 20–40 m depth flowing out of Lake Überlingen toward the main basin (Fig. 18, Fig. 17 on day 316.22). This is similar to records of Boehrer

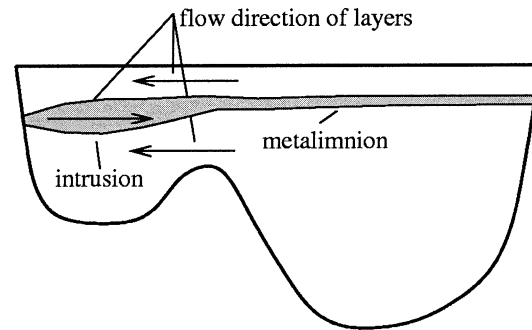


Fig. 18. Schematic of intrusion in Lake Überlingen.

et al. (2000). The Coriolis force deflected the intrusion to the southern shore as is seen in cross sections C2 and C1 (Fig. 14, day 316.22), while rapid cooling eroded the density stratification. The three-layer structure was again changed into a two-layer structure when the flow direction in the upper layer changed toward the main basin, while inflow into Lake Überlingen persisted.

The goal of the present study was to develop a coherent overview of the baroclinic basin-scale motions of a large lake with a complex geometry and nonuniform wind field. The coarse-grid three-dimensional numerical model ELCOM was shown to be capable of reproducing the dominant internal oscillations without lake-specific calibration. Periods, amplitudes, and phases of dominant internal waves were resolved down to periods of 8 h. A nonuniform wind field as model input appears to be significant in order to simulate the baroclinic basin-scale dynamics of this large lake, particularly the upwelling structure. This study made use of both field work and three-dimensional numerical modeling. Two examples for the benefit of this approach were given: first, combining field measurements with validated simulations allowed us to identify the local vertical velocity structure of internal waves, particularly to recognize a 14-h Poincaré-type wave of the second vertical mode. Second, it was possible to use simulated velocities for a quantitative analysis of force balances.

Typical strongest upwelling in Upper Lake Constance for westerly wind does not occur at the upwind end of the lake but near the interface of the subbasins, while part of the warmer surface layer still remains in Lake Überlingen. The width and length ratios of the subbasins, the wind chronology, and wind shadowing over Lake Überlingen, as well as the Coriolis force, seem to play significant roles in this. This particular upwelling behavior causes colder bottom water to reach the surface first east of the Sill of Mainau. Layers of warmer surface water in Lake Überlingen and in the main basin are thus split by this cold bottom water. Warmer water from the smaller subbasin flows on top of colder water when it is dragged across the interface into the main basin. This may result in an additional efficient mixing mechanism that is to be further explored. ELCOM runs with different seasonal temperature profiles suggest that the phenomenon of the split surface layer may frequently occur in the lake during strong westerly wind events.

The relaxation of the water body and the nonlinear Kelvin

wave were observed to be internal surges moving toward the northwestern end of Lake Überlingen. The internal surge and its reflection cause a two-step thermocline that can be easily distinguished in temperature profiles. It is thus a suitable indicator for the nonlinearity of the lake response such as suggested by field data by Schimmele (1993), Boehrer et al. (2000), Zenger (1989), and Kocsis et al. (1998). The two-step thermocline and the transition of the velocity field in Lake Überlingen from a two-layer velocity structure into a three-layer velocity structure are closely linked. The presented weak two-step thermocline around day 307 and a similar event during a period of days 293–303 in the year 1993 show strong quantitative similarities concerning the stratification and the wind forcing (Kocsis et al. 1998). This agreement may help to explain increased vertical diffusivities measured by Kocsis et al., since the observed two-step thermocline in their measurements indicates that the authors had measured the increased diffusivities when a weak internal surge had just passed the sill. Further analysis is suggested in this direction, since this may help to shed further light on mixing and transport processes in Upper Lake Constance and other large lakes of similar geometry.

References

- ANTENUCCI, J. P., AND J. IMBERGER. 2001. Energetics of long internal gravity waves in large lakes. *Limnol. Oceanogr.* **46**: 1760–1773.
- , ———, AND A. SAGGIO. 2000. Seasonal evolution of the basin-scale internal wave field in a stratified lake. *Limnol. Oceanogr.* **45**: 1621–1638.
- BÄUERLE, E. 1981. Die Eigenschwingungen abgeschlossener, zweigeschichteter Wasserbecken bei variabler Bodentopographie. *Berichte aus dem Institut für Meereskunde, Christian-Albrechts-Universität.*
- . 1994. Transverse baroclinic oscillations in Lake Überlingen. *Aquat. Sci.* **56**: 145–160.
- , D. OLLINGER, AND J. IMBERGER. 1998. Some meteorological, hydrological, and hydrodynamical aspects of Upper Lake Constance. *Arch. Hydrobiol. Spec. Issues Adv. Limnol.* **53**: 31–83.
- BENDAT, J. S., AND A. G. PIERSOL. 1971. *Random data: Analysis and measurement procedures.* Wiley-Interscience.
- BOEHRER, B., J. IMBERGER, AND K.-O. MÜNNICH. 2000. Vertical structure of currents in Western Lake Constance. *J. Geophys. Res.* **105**: 28823–28835.
- CSANADY, G. T. 1982. On the structure of transient upwelling events. *J. Phys. Oceanogr.* **12**: 84–96.
- FARMER, D. F. 1978. Observation of long nonlinear waves in a lake. *J. Phys. Oceanogr.* **8**: 63–73.
- GONELLA, J. 1972. A rotary-component method for analyzing meteorological and oceanographic vector time series. *Deep-Sea Res.* **19**: 213–231.
- HAYAMI, Y., T. FUJIWARA, AND M. KUMAGAI. 1996. Internal surge in Lake Biwa induced by strong winds of a typhoon. *Jpn. J. Limnol.* **4**: 425–444.
- HEINZ, G. 1995. *Strömungen im Bodensee. Ergebnisse einer Meskampagne im Herbst 1993, Vol. 135. Mitteilungen der VAW der ETH Zürich.*
- HODGES, B. R., AND C. J. DALLIMORE. 2001. *Estuary and lake computer model. ELCOM science manual code version 1.5.0. Centre for Water Research, University of Western Australia.*
- , J. IMBERGER, A. SAGGIO, AND K. B. WINTERS. 2000. Modeling basin-scale interval waves in a stratified lake. *Limnol. Oceanogr.* **45**: 1603–1620.
- HOLLAN, E. 1974. Wind-induced motions in Lake Constance. *Bericht der AWBR.* **6**: 111–187.
- HUNKINS, K., AND M. FLIEGEL. 1973. Internal undular surges in Seneca Lake: A natural occurrence of solitons. *J. Geophys. Res.* **78**: 539–548.
- HUSS, E., AND D. STRANZ. 1970. Die Windverhältnisse am Bodensee. *Pure Appl. Geophys.* **81**: 323–356.
- IMBERGER, J. 1998. Flux paths in a stratified lake: A review. *Coast. Estuar. Stud.* **54**: 1–18.
- , AND J. C. PATTERSON. 1990. Physical limnology. *Adv. Appl. Mech.* **27**: 303–475.
- KOCSIS, O., B. MATHIS, M. GLOOR, M. SCHURTER, AND A. WÜEST. 1998. Enhanced mixing in narrows: A case study at the Mainau Sill, Lake Constance. *Aquat. Sci.* **60**: 236–252.
- KUNDU, P. K. 1990. *Fluid mechanics.* Academic.
- LAVAL, B., B. R. HODGES, AND J. IMBERGER. 2003. Reducing numerical diffusion effects with a pycnocline filter. *J. Hydraul. Engin.* **129**: 215–224.
- , J. IMBERGER, B. R. HODGES, AND R. STOCKER. 2003. Modeling circulation in lakes: Spatial and temporal variations. *Limnol. Oceanogr.* **48**: 983–994.
- LEMMIN, U. 1987. The structure and dynamics of internal waves in Baldeggersee. *Limnol. Oceanogr.* **32**: 43–61.
- MORTIMER, C. H. 1952. Water movements in lakes during summer stratification: Evidence from the distribution of temperature in Windermere. *Philos. Trans. R. Soc. Lond. B* **236**: 355–404.
- . 1974. Lake hydrodynamics. *Mitt. Int. Ver. Limnol.* **20**: 124–197.
- , AND W. HORN. 1982. Internal wave dynamics and their implications for plankton biology in the Lake of Zürich. *Vierteljahresschrift Nat.forsch. Ges. Zürich* **127**: 299–318.
- MÜHLEISEN, R. 1977. Starkwinde an und auf dem Bodensee. *Meteorol. Rundsch.* **30**: 15–22.
- OLLINGER, D. 1999. *Modellierung von Temperatur, Turbulenz und Algenwachstum mit einem gekoppelten physikalisch-biologischen Modell.* Ph.D. dissertation, Ruprecht-Karls-Universität, Heidelberg.
- SCHIMMELE, M. 1993. *Anregung interner Seiches im Bodensee durch den Wind.* Ph.D. dissertation, Universität Heidelberg.
- THORPE, S. A. 1974. Near-resonant forcing in a shallow two-layer fluid: A model for the internal surge in Loch Ness? *J. Fluid Mech.* **63**: 509–527.
- , AND A. HALL. 1972. The internal surge in Loch Ness. *Nature* **237**: 96–98.
- WANG, Y., K. HUTTER, AND E. BÄUERLE. 2000. Wind-induced baroclinic response of Lake Constance. *Ann. Geophys.* **18**: 1488–1501.
- WESSELS, M. 1998. *Geological history of the Lake Constance area.* *Arch. Hydrobiol. Spec. Issues Adv. Limnol.* **53**: 1–12.
- ZENGER, A. 1989. *Ursachen und Auswirkungen von Transport- und Mischungsprozessen im westlichen Bodensee.* Ph.D. dissertation, Universität Heidelberg.
- , W. ANKER, J. IMBERGER, AND K.-O. MÜNNICH. 1990. Die Untersuchung der Windverhältnisse im westlichen Teil des Bodensees und die Untersuchung von Landwinden auf Seebedingungen. *Meteorol. Rundsch.* **42**: 42–51.
- , J. IMBERGER, G. HEINZ, M. SCHIMMELE, AND K.-O. MÜNNICH. 1989. *Untersuchung der Struktur der internen Seiches des Bodensees.* *Wasserwirtschaft* **79**: 616–623.

Received: 15 January 2003
Accepted: 30 January 2004
Amended: 2 March 2004